Aachen Institute for Advanced Study in Computational Engineering Science

Preprint: AICES-2009-3

30/January/2009

Phase-field simulations of free-volume growth in eutectic colonies with coupled heat and solute diffusion

Z. Ebrahimi, J. L. Rezende, J. Schöberl

RWTH AACHEN UNIVERSITY

AICES

Financial support from the Deutsche Forschungsgemeinschaft (German Research Association) through grant GSC 111 is gratefully acknowledged.

List of AICES technical reports: http://www.aices.rwth-aachen.de/preprints

Phase-field simulations of free-volume growth in eutectic colonies with coupled heat and solute diffusion

Z. Ebrahimi, J. L. Rezende and J. Schöberl

AICES Institute, RWTH Aachen, D-52056 Germany
Institute of Minerals Engineering (GHI), RWTH Aachen, D-52056 Germany
Center for Computational Engineering Science (CCES), RWTH Aachen, D-52056 Germany

Abstract

A quantitative phase-field model is used to investigate the free-volume microstructural pattern formation of eutectic colonies with coupled heat and solute diffusion. The effects of thermal diffusity on morphological instability wavelength in free-growth are formulated by simulating the dynamics of fully developed colonies. We find a good overall agreement with the experiments which show the formation of eutectic colonies in Ti-based alloys. The two-dimensional simulations show that the eutectic front dynamic happens on a scale much larger than the lamellar spacing and the evolution of the interface leads to the formation of fully developed lamellar sectors. The model reduces to the traditional sharp-interface model in a thin-interface limit, where the microscopic interface width is small but finite. Finally the model results are compared with isothermal free-volume growth.

Key words: Eutectic colonies; Phase-field model; Free-growth; Thermal diffusion

1. Introduction

Eutectic alloys are of interest to metallurgists because of their low melting points and of the superior mechanical properties associated with a fine-scale composite microstructure. Eutectic morphologies form when two or more phases grow simultaneously from the liquid. Due to the fact that they are composed of more than one phase, eutectics can exhibit a wide variety of geometrical arrangements [4, 6, 10]. The vast majority of technological useful eutectic alloys are composed of two phases. Therefore only the later type of eutectic will be considered here.

In alloy solidification, the solidification rate is limited by both heat and solute transfer. Heat transfer during solidification of an eutectic system can be treated using different possible approaches. Some phase-field simulations that assume coupled heat and solute diffusion at the interface have been reported [5, 12]. In these cases the heat and solute fields are coupled at the solid-liquid interface by the relations for the interface temperature and by heat and solute flux balances. In general the solutal diffusivity in the liquid state is generally two to four orders of magnitude smaller than the thermal diffusivity. Therefore, solute diffusion is often on a length scale similar to that of the microstructure, and small solute additions can strongly affect the interface pattern evolution [5]. However, for small concentrations even though the thermal diffusivity may be much larger than the solutal diffusivity, the solutal and thermal effects are still comparable and the solute and heat conservation equations need to be solved simultaneously. Some of the other numerical studies of eutectic solidification have omitted to solve heat equation, but employed other assumptions for temperature [9, 11].

Numerous experiments and numerical studies on directional solidification, where the samples are pulled from a hot into a cold region with a constant velocity, have attempted to investigate the eutectic front behavior including the lamellar spacing and pattern wavelength (λ) selection, as the interface undergoes various instabilities and exhibits some nonlinear features such as bifurcations [15, 18]. In an attempt to formulate a theory for wavelength selection in eutectic growth, an approximate potential function for λ has been derived and it has argued that under finite amplitude of noise, the wavelength selection on average is determined by a balance in the creation rates and annihilation rates of lamellae [15]. Amplitude equations that describe how the bifurcation effects create a tilted domain, have been derived in [17] and the dynamical wavelength selection mechanism have been predicted. It has been found that the selected wavelength should scale as $\lambda \sim \sqrt{ld} f(l/l_T)$, where a scaling function f depends on the diffusion and thermal lengths, l and l_T, respectively and d is the capillary length [16]. A phase-field study of ternary eutectics, which has shown how the presence of the third component in the system with an imposed thermal gradient leads to the formation of eutectic colonies and provided an effective description of the eutectic front on length scales much larger than the lamellar spacing, is reported in [8].

The phase-field approach has emerged as a powerful method to model the interfacial pattern formation and phase transition in a range of different systems and has been the subject of many researches recently [1, 2, 3, 4]. Its advantage to the traditional free-boundary problem (FBP) for predicting the interfacial growth is that discretizing and tracking of the sharp-boundaries is avoided by introducing additional continuum field variables (phase-field variables). The phase-field variables take constant values in each bulk phase and vary smoothly in a diffuse interface region of thickness W. In the so-called sharp-interface limit the phase-field equations reduce to the standard FBP as the interface thickness tends to zero.

Multiphase problems such as eutectic and peritectic phase formation can be examined using the phase-field method with multiple order parameters [6, 20]. In the context of the present work, we examine the system of coupled heat and solute diffusion by solving the heat equation together with phase-field and concentration fields to simulate the free-volume eutectic colonies formation. Experiments have widely shown that a steady-state lamellar eutectic solidification front is destabilized on a scale much larger than the lamellar spacing and forms two-phase cells commonly referred to as eutectic colonies [8]. These phenomena are investigated here by using a phase-field model for binary eutectic alloys. In this paper we extend a quantitative phase-field model of eutectic solidification [4] to work in the free volume for a given initial nucleus. At this point it is sufficient to calculate growth incorporating a single crystal orientation. The simulations predict both the radial and circumferential growth of the colonies. To model the instabilities leading to eutectic colonies formation, one requires to include stochastic noises in the system. We investigate by dynamical phase-field simulations the nonlinear evolution of the two-phase interfaces, which are a consequence of the interface instabilities. The simulation results show that the eutectic front dynamic happens on a scale much larger than the lamellar spacing and depends directly on Lewis numbers (the ratio of the thermal to the solutal diffusion coefficients). The nonlinear interface evolution leads to formation of fully developed two-phase sectors with a spacing much larger than the lamellar spacing. This large-scale envelope of the composite eutectic front exhibits tip-splitting events as the nucleus grows and converges to a steady state.

In the following section, we introduce the basic equations of free-boundary problem. The application of the phase-field method to free-volume eutectic growth is presented in Section 3 and the simulation results are then discussed in Section 4. Finally major results are summarized in Section 5.

2. Free-Boundary Problem

Consider the solidification of a binary alloy. We denote the two phases by α and β. The composition variation among the coexisting phases can be characterized by a concentration field, C and the concentration limits of the eutectic plateau, C_α and C_β. The composition and temperature of the eutectic point are denoted by C_E and T_E, respectively.

In free-volume eutectic colonies formation, the growth starts from a small seed of one and/or both phases in a large supercooled melt at a specified composition C_0 and temperature T_0. For the free-volume growth with coupled heat and solute diffusion, the temperature field in solid and liquid phases is given by the heat diffusion equation,

$$\partial_t T = \alpha \nabla^2 T \tag{1}$$

where the thermal diffusivity (α) is assumed to be equal in solid and liquid phases. The temperature of the solid-liquid interfaces is given by Gibbs-Thomson condition,

$$T = T_E + m_i(C_l - C_E) - \Gamma\kappa - v_n/u_i \tag{2}$$

where C_l is the concentration on the liquid side of the interface, T is the temperature field, κ is the local curvature of the interface, v_n is the interface normal velocity and $i = \alpha, \beta$. The liquidus slopes of the alloy phase diagram, m_i, are taken at the eutectic point, u_i are the kinetic coefficients and Γ is the Gibbs-Thomson coefficient defined as

$$\Gamma = \frac{\gamma_{iL} T_E}{L_i} \tag{3}$$

where γ_{iL} are the solid-liquid surface tensions and L_i are the latent heats. The solute transport occurs by diffusion and γ_{iL} are assumed to be isotropic here. The interface velocity and diffusion flux on the liquid side are related in a way that the total mass is conserved,

$$C_l(1 - k_i)v_n = -D\partial_n C_l \tag{4}$$

We define the dimensionless temperature as

$$\theta = \frac{(T - T_E)}{\tilde{L}/c_p} \tag{5}$$

where $\tilde{L} = 1/2(L_\alpha + L_\beta)$ is the average latent heat and c_p is the specific heat at constant pressure that is assumed equal for solid and liquid phases. The free-boundary problem in terms of θ and the scaled concentration field, $c = (C - C_E)/\triangle C$, becomes

$$\partial_t c = D\nabla^2 c \tag{6}$$

$$\partial_t \theta = \alpha \nabla^2 \theta \tag{7}$$

$$c_l(1 - k_i)v_n = -D\partial_n c_l \tag{8}$$

$$v_n = \alpha(\partial_n \theta_s - \partial_n \theta_l) \tag{9}$$

$$c_i - Y\theta_i = d_i\kappa - \beta_i v_n \tag{10}$$

where $Y = \tilde{L}/(c_p m_i \triangle C)$ and $\triangle C = C_\beta - C_\alpha$. In these equations, d_i and β_i are the thermal capillary lengths and kinetic coefficients, respectively.

$$d_i = \frac{\Gamma}{|m_i|\triangle C} = \frac{\gamma_{iL} T_E}{|m_i|\triangle C L_i} \tag{11}$$

$$\beta_i = \frac{1}{u_i |m_i| \triangle C} \tag{12}$$

One should note that the subscript i on θ and c represents the quantities being evaluated at the interface.

3. Phase-Field Modeling Approach

In this section we formulate a phase-field model of growth in eutectic colonies for a class of binary alloys that involves a single liquid and two solid phases. To develop a phase-field model for two-phase solidification, a smooth free-energy functional can be defined specifically to ensure the absence of the third phase in the interfaces. This free-energy functional provides a coupling between concentration and the phase-field variables.
The phase-field model is not treated themodynamically here. Therefor the free-energy functional takes the form of the Helmholtz free energy for the given free-boundary problem (FBP). The model that we describe here is capable to accommodate arbitrary eutectic phase diagrams and reduces to the standard phase-field model of single order-parameter, for each of the two solid-liquid interfaces. This mapping allows us to deduce the thin-interface behavior of the two-phase interfaces without performing a detailed asymptotic analysis [4].

The phase-field method for a multiphase system begins by assigning a seperate field p_i to each phase ($i = \alpha, \beta, L$), each of which is unity in the corresponding ith single phase region ($p_i = 1$) of the sample and zero outside that phase ($p_i = 0$). Each phase-field parameter can then be understood as a local volume fraction such that $\sum_i p_i = 1$ and $0 \leqslant p_i \leqslant 1$. We assume that on a interface connecting phases i and j, no other phase is present ($p_k = 0,\ k \neq i, j$). In order to construct the phase-field model, we introduce a free-energy functional that provides the thermodynamic features of the phase transformation. We formulate the total free energy as a functional of the field variables, which is defined as the volume integral of a free-energy density f.

$$F = \int_V f dV \tag{13}$$

In other words, the chemical free energy as a function of field variables can be approximated as a free-energy functional, which is the volume integral of a free-energy density $f(\vec{p}, c, T)$,

$$f(\vec{p}, c, T) = \frac{1}{2}\sum_i (\nabla p_i)^2 + H f_p(\vec{p}) + f_c(c, T, \vec{p}) \tag{14}$$

where f_p is the potential term of the free-energy density and depends only on the phase field, f_c defines the basic thermodynamic properties of the system and couples the phase field to the concentration and temperature (see Eq. (3.19) in Ref. [4]) and H is a constant term. The temporal evolution of the concentration field is described by solute diffusion equation,

$$\frac{\partial c}{\partial t} = \nabla . \left(M(p_i) \nabla \frac{\delta F}{\delta c} \right) \tag{15}$$

where $M(p_i)$ are the diffusional mobility terms. We define the chemical potential to simplify the solute diffusion equation,

$$\mu = \frac{\delta F}{\delta c} = \frac{\partial f}{\partial c} = c - \sum_i A_i(T) h_i(\vec{p}) \tag{16}$$

The $A_i(T)$ and $B_i(T)$ are obtained by linearization of the phase diagram around the eutectic point as specified in [4]. The function $h_i(\vec{p})$ should have the value one in each bulk phase and zero otherwise ($h_i(p_i = 1) = 1$ and $h_i(p_i = 0) = 0$). Here we choose $h(p_i) = p_i$, which make it possible to use a coarser discretization for saving some computational costs.

In a typical metallic alloy system the solid phases have a diffusion coefficient which is approximately four orders of magnitude smaller than its value in the liquid phases. Here we choose the solid diffusion coefficient in such a way that its ratio to liquid diffusion constant is of order 10^{-2},

$$\tilde{D_s} = \frac{D_s}{D_L} \tag{17}$$

where $s = \alpha, \beta$ for a binary system and D_s and D_L are assumed constant here. Although we have not assumed zero solid diffusion coefficient, but the solid diffusivity is much less than that in the liquid and the model is one-sided. Therefore the antitrapping current has been added to the continuity equation to counterbalance the physical solute trapping effects [4]. The antitrapping current counterbalances the solute effects when a mesoscopic interface thickness is used to simulate the interface evolution on experimental length and time scale. By substituting the chemical potential given by Eq. (16) in Eq. (15) the continuity equation becomes

$$\frac{\partial \mu}{\partial t} = \vec{\nabla} . \left(D(\vec{p}) \vec{\nabla} \mu - \vec{j}_{at} \right) \tag{18}$$

where $D(\vec{p}) = \sum_j D_j p_j$, D_j represents the diffusion coefficient of the phase labeled j and $\vec{j}_{at}$ is the antitrapping term. The spatial-temporal evolution of these field variables defines the evolution of an arbitrary microstructure. In this context two coupled non-linear partial differential equations describe the evolution of the interface and the equilibrium front problem.

$$\tau(\vec{p}) \frac{\partial p_i}{\partial t} = -\frac{1}{H} \frac{\delta F}{\delta p_i} |_{\sum_i p_i = 1} + \eta_i \quad \forall i \tag{19}$$

where $\tau(\vec{p})$ is a relaxation time and η_i are the stochastic noise terms that are related to the interface instabilities. By use of the Lagrange mulitipliers, the variational formulation can be formulated as

$$\frac{\delta F}{\delta p_i}|_{\sum_i p_i=1} = \frac{\delta F}{\delta p_i} - \frac{1}{3}\sum_j \frac{\delta F}{\delta p_j} \tag{20}$$

$$\frac{\delta F}{\delta p_i} = \frac{\partial f}{\partial p_j} - \sum_\nu \partial_\nu \frac{\partial f}{\partial(\partial_\nu p_i)} \tag{21}$$

where ν denotes the spacial coordinates. To perform the variation on the r.h.s of Eq. (20), p_i are assumed to be independent. As we metioned before, the i-j interface should be free of the other phases. This requirement ensures that with appropriate initial and boundary conditions, p_i are always between 0 and 1, $p_i \in [0,1]\ \forall i$. At an equilibrium state, the variational derivatives of F must satisfy the following conditions

$$\frac{\delta F}{\delta p_i}|_{\sum_i p_i=1, p_k=0,1} = 0 \quad \forall(i,k) \tag{22}$$
$$\frac{\delta^2 F}{\delta p_i^2}|_{\sum_i p_i=1, p_k=0,1} > 0 \quad \forall(i,k)$$

The first condition not only ensures the absence of the third phase absorbtion, but also the two wells of every pure i-j interface remain at $p_i = 0, 1$ in spite of the move of the interface.

3.1. Coupled Heat and Solute Diffusion

Here, we write down the evolution equations for free-volume eutectic colonies formation, in which the heat and concentration fields are coupled at the solid-liquid interfaces. The stochastic noises should be included in the eutectic system to simulate fluctuations at the interface, which are necessary to model most of the eutectic structures observed in real systems. These noise terms allow heterogeneous nucleation leading a system from a metastable state to a stable state. To model the noise we introduce an additional phase-dependence term into the phase-field equations,

$$\eta_i = R_i(t)M_i p_j(1-p_j) + R_L(t)M_L p_L(1-p_L) \quad (i \neq j) \tag{23}$$

where R_i and $R_L(t)$ are random numbers between zero and one, M_i and M_L are the magnitudes of the fluctuation and p_L is the phase-field variable for the liquid phase. One should note that here we have used a simple method to include the fluctuation effects. However a more rigorous method of introducing noise is possible, i.e. assuming Langevin random noise [19].

To derive the heat transfer equation, we introduce the internal energy density e as a conserved variable. The evolution of e can be governed by the normal conservation law for internal energy,

$$\dot{e} = -\nabla.J_e \tag{24}$$

where J_e is the heat flux given by

$$J_e = L_e \nabla \frac{\delta F}{\delta e} \tag{25}$$

The coefficient L_e is related to the heat conduction. The temperature evolution equation for a free eutectic growth can be written as,

$$\frac{\partial T}{\partial t} = \alpha \nabla^2 T + \sum_i \frac{L_i}{c_p}|A_L - A_i|\frac{\partial p_i}{\partial t} \tag{26}$$

The phase-field evolution equation in terms of dimensionless temperature θ, is obtained by substituting the free-energy density given by Eq. (14) in Eq. (19).

$$\tau(\vec{p})\frac{\partial p_i}{\partial t} = W^2\nabla^2 p_i + \frac{2}{3}[-2p_i(1-p_i)(1-2p_i) + \sum_{j\neq i} p_j(1-p_j)(1-2p_j)] + \bar{\lambda}\sum_j \frac{\partial g_i}{\partial p_i}|_{\sum_i p_i=1}(c_i + (k_i-1)Z_i\theta)(\mu - Z_i\theta) + \eta_i \quad \forall i \tag{27}$$

where $Z_i = \mp\tilde{L}/(c_p m_i \triangle C)$ are constant terms and the function g_i is given by Eq. (3.17) in Ref. [4]. Assuming constant solid and liquid diffusion coefficients, the equation for solute concentration reads

$$\frac{\partial \mu}{\partial t} = \vec{\nabla}.\left(\sum_i (D_i p_i)\vec{\nabla}\mu\right) - \sum_i (A_i\frac{\partial p_i}{\partial t} + (k_i-1)Z_i\frac{\partial \theta}{\partial t}) + 2a\sum_{i=\alpha,\beta}(A_i - A_L)(-\hat{n}_L.\hat{n}_i)\vec{\nabla}.\left(\hat{n}_i\frac{\partial p_i}{\partial t}\right) \tag{28}$$

where $A_i = c_i + (k_i-1)Z_i\theta$. The coefficients k_i are partition coefficients which relate the concentrations on the solid and liquid side of the interfaces, $k_i = C_s/C_l$.

4. Numerical Simulations

In the following we present the numerical solutions of the phase-field model derived in the preceding section to study the free-volume eutectic colonies formation. The goal is to study the dynamic behavior of free colonies formation and to investigate the effects of the heat diffusion. The evolution equations are discretized using a finite difference method on a uniform rectangular mesh. The explicit Euler scheme is used for the time stepping. To carry out the simulations, it is useful to define the scaled diffusivity, $\bar{D} = D\bar{\tau}/W^2$, and relaxation time, $\bar{\tau}(\vec{p}) = \tau(\vec{p})/\bar{\tau}$, by using $\bar{\tau}$ and W as the time and length scales. For computational efficiency, we use a symmetric eutectic phase diagram in

which $|m_\beta| = |m_\alpha| = m$, $|c_\beta|/|c_\alpha| = 1$, $\tilde{L} = L_\alpha = L_\beta$ and $k_\alpha = k_\beta = 1$. The initial composition of each solid phase is set to its equilibrium composition at the eutectic temperature, -0.5 and 0.5 for c_α and c_β. The liquid diffusion coefficient D and the average capillary $\bar{d}$ length are set to $0.5 \times 10^{-9}\ m^2/s$ and $6.5\ nm$, respectively.

4.1. Simulations of Thermosolutal Free-Volume Solidification

In free eutectic growth with coupled heat and solute diffusion, as the morphology evolves, the thermal and solutal diffusions proceed in different time scales and the length scales of both processes also differ. To obtain the domain independent solution for free eutectic growth (having eutectics growing freely), the computational domain should be large enough to prevent significant effects of the boundary on the results. Otherwise the eutectic growth will be constrained in a small box with a constant wall temperature or cooling rate and the results will be domain dependent. In other words, the selected domain should be large enough for a thermal boundary layer, which is about four orders in magnitude larger than the solutal one. On the other hand, one should note that the numerical mesh is fine enough for the interface and solutal fields. We choose a square domain with symmetric boundary conditions applied on the bottom and left boundaries and no-flux boundary conditions on the right and top sides. The eutectic growth starts from a small seed of one and/or both phases in a large supercooled melt at a specified composition c_0 and temperature T_0. The Lewis number is defined as the ratio of the thermal to the solutal diffusion coefficient, $Le = \alpha/D$. The radius of the initial circular solid seed is $10d_\alpha$ for all runs. The grid spacing is chosen as $\triangle\bar{x} = \triangle x/W = 0.8$ and the minimum time step is varied depending on D, Le or $\bar{\lambda}$. The only truly free computational parameter is now the interface thickness, W that is chosen according to our model parameters. Hence, the resolution of the phase-field simulations is given by the ratio $W/\bar{d}$ or by $\bar{\lambda}$. The computational domains are adjusted to have the same physical size in each case.

First, simulations for $Le = 1$ are performed. Fig. (1) shows the simulation results of free-volum growth with one nucleus. The initial dimensionless undercooling and the coupling constants are chosen as $\triangle = 0.55$ and $\bar{\lambda} = 18.19$. The governing equations are solved on a grid of 600×600 node points with grid size and the time step equal to 0.8 and 0.021, respectively. The magnitude of the noise coefficients, M_α and M_β, are set to 0.4 and 1.0 for this simulation. The two solid phases α and β are represented as tree-like structures with different colors in Fig. (1.a). The initial quarter-circular seed of α phase placed at lower-left corner grows into a slightly undercooled melt. The whole structure is then obtained by reflection of this configuration about the $x = y = 0$ lines. It can be seen from the simulation results that at the solid-liquid interfaces, some concave hollows are formed and the eutectic microstructure evolves in a tree-like structure. The solid particles of one phase nucleate on the opposite phase within the concave portion of the interfaces. Consequently some eutectic lamellae (α or β) appear through this kind of nucleation and some disappear by the suppression of the neighboring lamellae. Jackson and Hunt found no experimental evidence for the reduction of lamellae spacing by nucleation of new lamellae, in the case of a too wide value of this spacing under the corresponding processing condition, which brings about growth instabilities [14]. Nevertheless, some authors have argued that this nucleation mechanism may play a role in the stabilization of the lamellae spacing value [6, 21, 22].

The bifurcation effects are represented with light color points in Fig. (1.b), and show the position of initiation of the second phase (β or α) on the valley of the first phase, while both α and β phases are presented in the same color. It is observed also that the bifurcation effects appear on a series of circular paths originated from the initial seed, at lower-left corner, as the lamellae grow. These periodicity-increasing bifurcations give rise to localized tilted domain and enlarge the space of the possible stationary solution in the radial growth.

Another interesting observation in the performed simulations, is the formation of fully developed petal-like sectors comprising of the lamellae of both phases, which initiate from the origin seed as the lamellar structure grows. The eutectic system selects a wavelength λ by adjusting the creation and the annihilation rates of the lamellae. It is observed that this wavelength is much larger than the distance between two neighbor lamellae of different phases (lamellar spacing ξ) and depends on the thermal and solutal diffusion coefficients and the amount of perturbations adding on the interfaces. In other words, the eutectic front dynamic happens on a scale much larger than the lamellar spacing which is determined by the Lewis numbers of the eutectic system. Therefore the geometry of the lamellar interface is determined by both the interlamellar and thermal diffusion lengths. This large-scale envelope of the composite eutectic front exhibits tip-splitting events as the nucleus grows and the microstructure converges to a steady state.

The tip-splitting phenomena are shown more precisely in Fig. (2.a), where three distinct petal-like sectors are marked. The overall geometry spacing is defined as the distance between two fully developed non-splitting sectors (eutectic front wavelength λ). The α and β phases are presented as light and dark color structures. This run is performed on a lattice of size 1000×1000 with the same undercooling and the material parameters as the previous simulation. The noise coefficient M_β is 0.6 for this simulation. Fig. (2.b) shows that the number of the petal-like sectors are increased periodically as the morphology

evolves to a steady state. These phenomena can be understand by considering the fact that λ, which is determined by both thermal and solutal diffusion lengths, is constant for a specific run . On the other hand as the microstructure grows, the circumference of the outer circle of geometry increases and the lamellar sectors initiated in the previous time steps can not cover it. Therefor the system needs always to initiated new lamellar sectors to stabilize. A good overall agreement between simulations and experiments can be found by visualization of the simulation results for two nuclei, Fig. (3).

4.2. Effects of the Thermal Diffusion on Free-Growth

In order to investigate the effects of including the thermal diffusion field on the eutectic free-growth, a series of simulations have been conducted. First we perform the simulation of isothermal free-growth with a constant cooling rate $\delta = 0.015$. The simulation domain is a square of 600×600 nodal points with a grid spacing of $\Delta x = 0.8$ and a time step of $\Delta t = 0.02$. The model parameters are chosen the same as the previous runs. The predicted results for the phase-field variables are presented in Fig. (4). Comparing this with the results of thermosolutal growth with $Le = 1$, Fig. (1.a), shows that in the isothermal free-growth, the radial structure is more uniform and the petal-like sectors are not formed on the eutectic front. Therefor for the modeling of the eutectic colonies formation in free-growth in a computationally efficient way, one needs to couple the thermal diffusion equation with the concentration field and the phase-field equations.

Another study has been done to establish the influence of the thermal diffusion on the eutectic growth by comparing the simulation results with different Lewis numbers. The time-steps are adjusted according to the stability limits of the discretized heat and concentration diffusion equations, $\triangle\bar{t} = (1/4)(\triangle x/W)^2 min\{1/\bar{D}, 1/\alpha, \bar{\tau}_\alpha, \bar{\tau}_\beta\}$. The computational domain should be large enough to fulfill the condition of domain independency. The computed front wavelength with respect to the lamellar spacing λ/ξ are 14, 18 and 20 for $Le = 1$, $Le = 2$ and $Le = 4$, respectively. Since the concentration diffusion coefficient were kept constant in the whole simulations, one can conclude that as the heat diffusion coefficient becomes larger, the wavelength λ increases and larger petal-like sectors will form. However to formulate a more precise relation for the wavelength λ more detailed studies are required.

5. Conclusion

In this paper we have presented a quantitative phase-field model to investigate the free-volume microstructural pattern formation of eutectic colonies with coupled heat and solute diffusion. First we have extended the phase-field model of directed eutectic solidification [4] to work in the free volume for a given initial nucleus. At this point it was sufficient to calculate growth incorporating a single crystal orientation. The model reduces to the traditional sharp-interface model in a thin-interface limit, where the microscopic interface width is small but finite. Then we have examined the system of coupled heat and solute diffusion by solving the heat equation together with phase-field and concentration field equations to simulate the free-volume eutectic colonies formation. This model has enabled us to simulate the tree-like lamellar structures of eutectic colonies for binary alloys.

To model the instabilities leading to eutectic colonies formation, stochastic noises were included in the system. We have investigated by dynamical phase-field simulations the nonlinear evolution of the two-phase interfaces. The periodicity-increasing bifurcations have been observed during the simulations on a series of circular paths through the lamellar structure with an origin on the initial seed. These bifurcations have tilted the domain and enlarged the space of the stationary solution in the radial growth.

Another interesting observation in the performed simulations was the formation of fully developed petal-like sectors comprising of the lamellae of both phases during the growth of the eutectic structures. We observed that the eutectic system selects a wavelength λ by adjusting the creation and the annihilation rates of the lamellae. The calculated wavelength was much larger than the lamellar spacing which was in a good agreement with the previous study on directed eutectic colonies formation [8]. Furthermore we found that λ depends on the thermal and solutal diffusion coefficients and the amount of perturbations adding on the interfaces. As a conclusion, the eutectic front dynamic happens on a scale much larger than the lamellar spacing which is determined by the Lewis numbers of the eutectic system. Therefore the geometry of the lamellar interface is determined by both the interlamellar and thermal diffusion lengths. The simulation results have shown also that the number of the petal-like sectors formed on the large-scale envelope of eutectic front, were increasing periodically as the morphology evolved to a steady state. These phenomena could be understood by considering the fact that λ, which was determined by both thermal and solutal diffusion lengths, has been kept constant for a specific run. On the other hand as the microstructure was growing, the circumference of the outer circle of geometry has increased, so that the lamellar sectors initiated in the previous time steps could not cover it. Therefor the system needed always to initiate new lamellar sectors to stabilize.

We have also compared the model results of thermosolutal free-growth with isothermal free-volume growth. In the case of isothermal free-growth, the radial structure was more uniform and the petal-like sectors were not formed on the eutectic front. Therefor for the modeling of the eutectic colonies formation in free-growth in a computa-

tionally efficient way, it was necessary to couple the thermal diffusion equation with the concentration field and the phase-field equations. Another study has been carried out to establish the influence of the thermal diffusion on the eutectic growth by performing a series of simulations with different Lewis numbers. The concentration diffusion coefficient and other physical parameters were kept constant for the whole runs. We saw that as the heat diffusion coefficient became larger, the wavelength λ has increased and larger petal-like sectors have been formed. However to formulate the relationship of the wavelength λ and the solutal and thermal diffusion lengths precisely, an additional parameter study is required.

Acknowledgments

Financial support from the Deutsche Forschungsgemeinschaft (German Research Association) through grant GSC 111 is gratefully acknowledged. We thank R. Siquieri for useful discussions about the model in Ref. [4].

References

[1] R. Kobayashi, Physica D 1993; **63**: 410
[2] A. Karma and W. J. Rappel, Phys. Rev. E 1998; **57**: 4
[3] J. L. Rezende and P. R. Sahm, Scripta. Mater. 1998; **38**: 157
[4] R. Folch and M. Plapp, Phys. Rev. E 2005; **72**: 011602
[5] J.C. Ramirez, C. Beckermann and A. Karma, Phys. Rev. E 2004; **69**: 051607
[6] B. Nestler and A. A. Wheeler, Physica D 2000; **138**: 114
[7] M. Plapp and A. Karma, Phys. Rev. E 2002; **66**: 061608
[8] M. Plapp and A. Karma, Phys. Rev. E 1999; **60**: 6865
[9] J. A. Warren and W. J. Boettinger, Acta. Mater. 1995; **43**: 689
[10] W.J. Boettinger, J.A. Warren, C. Beckermann and A. Karma, Annu. Rev. Mater. 2002; **32**: 163
[11] I. Loginova, G. Amberg and J. Agren, Acta. Mater. 2001; **49**: 573
[12] C. W. Lan, Y. C. Chang, and C. J. Shih, Acta. Mater. 2003; **51**: 1857
[13] A. Karma and A. Sarkissian, Met. Trans. A 1996; **27**: 635
[14] K. A. Jackson and J. D. Hunt, Trans. Metall. Soc. AIME 1966; **236**: 843
[15] V. Datye and J.S. Langer, Phys. Rev. B 1981; **24**: 4155
[16] K. Kassner, C. Misbah, Phys. Rev. Lett. 1991; **66**: 1551
[17] R. Baumann, K. Kassner, C. Misbah, D. Temkin, Phys. Rev. Lett. 1995; **75**: 2445
[18] M. Ginibre, S. Akamatsu, and G. Faivre, Phys. Rev. E 1997; **56**: 780
[19] A. Artemev, Y. Wang and A. G. Khachaturyan, Acta. Mater. 2000; **48**: 2503
[20] I. Steinbach, F.Pezzolla, B. Nestler, J. Rezende, M. Seesselberg and G. J. Schmitz, Physica D 1996; **94**: 135
[21] S. T. Bluni, M. R. Notis and A. R. Marder, Acta. Metall. Mater. 1995; **43**: 1775
[22] M. F. Zhu and C. P. Hong, Phys. Rev. B 2002; **66**: 155428
[23] J. Das, K. B. Kim, F. Baier, W. Löser and J. Eckert, Appl. Phys. Lett. 2005; **87**: 161907

List of Figures

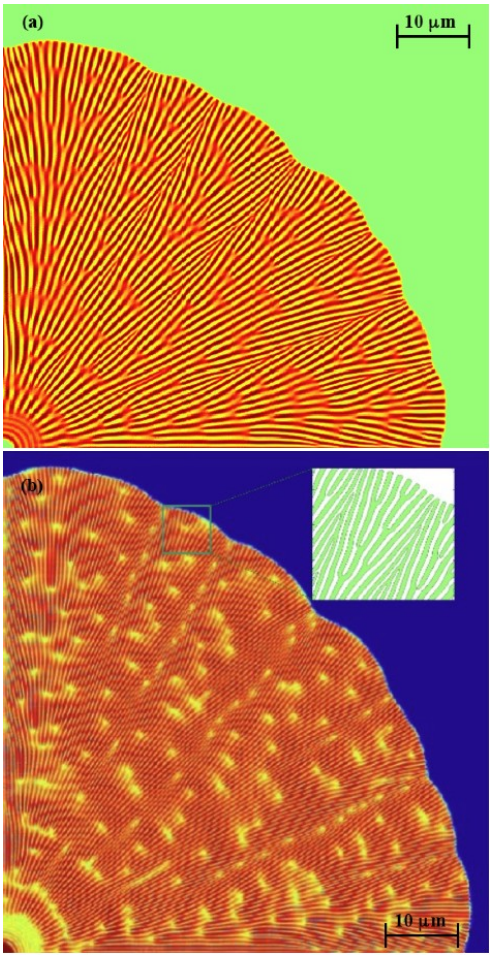

Figure 1: Free-volume eutectic colonies formation of one nucleus showing lamellar structures (a) and bifurcation effects (b).

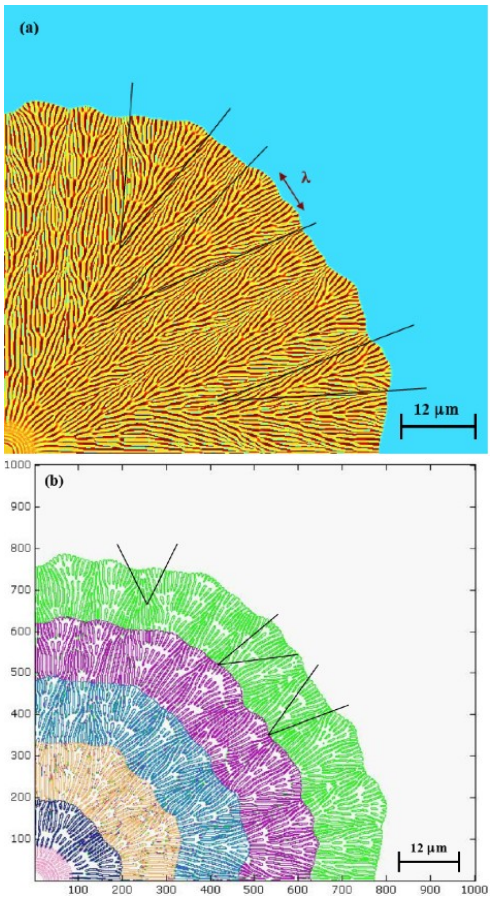

Figure 2: A fully developed eutectic colony, in which several tip-spliting envelopes are observed (a) and contour plots of microstructure after each certain number of cycles (some of the tip-splitting areas are marked) (b).

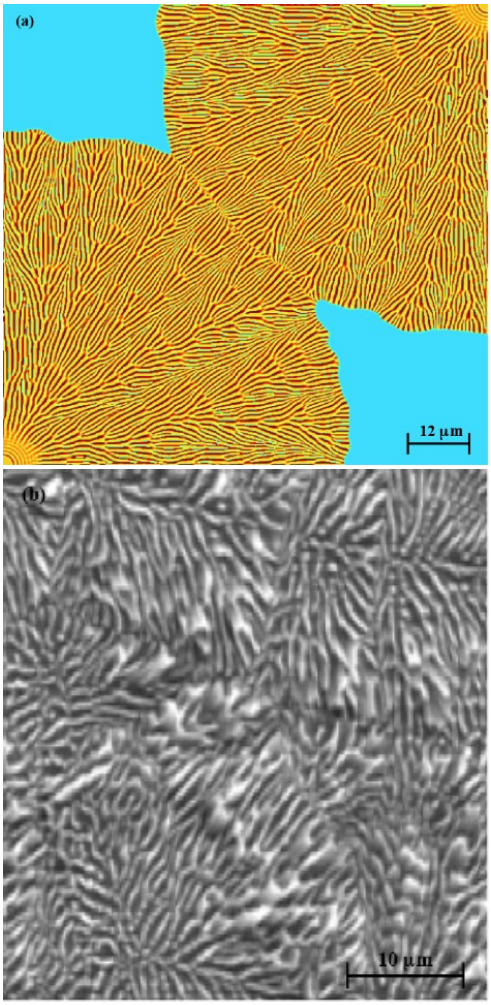

Figure 3: A qualitative comparison between simulation results and experiments. Phase-field simulation of eutectic colonies for a symmetric alloy of two nuclei (a) and experimental eutectic colonies of Ti-Fe observed in [23] (b).

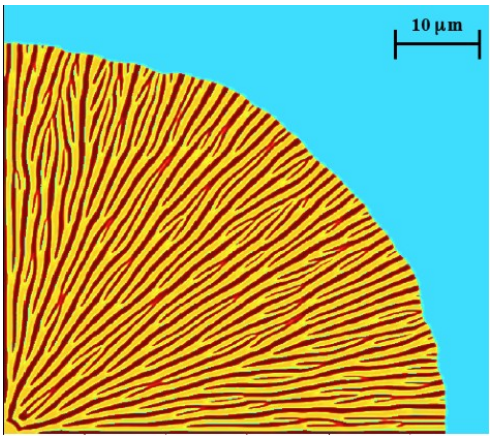

Figure 4: Isothermal eutectic free-growth with constant cooling rate $\delta = 0.015$.